文章编号 2095-1531(2020)02-0411-15

Optimization design and experimental study of micro-Fourier transform spectrometer

ZHAO Yun[1,2], LV Jin-guang[1*], QIN Yu-xin[1], TAO Jin[1], LIANG Zhong-zhu[1], WANG Wei-biao[1], NI Qi-liang[1], MENG De-jia[1], LIANG Jing-qiu[1*]
(1. *Changchun Institute of Optics, Fine Mechanics and Physics, Chinese Academy of Sciences, Changchun* 130033, *China*;
2. *University of Chinese Academy of Sciences, Beijing* 100049, *China*)
* *Corresponding author, E-mail: jinguanglv@163.com; liangjq@ciomp.ac.cn*

Abstract: In order to achieve the goal of miniaturization and light weight of Fourier transform spectrometer, a light-weight grid beam splitter structure was designed instead of the traditional parallel plate beam splitter. The influence of the grid edge of the grid beam splitter on spectrum reconstruction was analyzed, and the tolerance of production error was proposed. The micro-Fourier transform spectrometer was modeled and simulated, and the optimal structure of the grid beam splitter was obtained. The spectral inversion was performed by system simulation, and the restored spectrum was obtained. The spectral error introduced by the grid beam splitter was calculated. The construction and debugging of the prototype was completed, and the recovered spectrum of the actual system was obtained, which proved the feasibility of the miniaturized system. Compared with the traditional Fourier transform spectrometer, the miniaturization system has the advantages of small volume and good stability, and can be used for online monitoring.

Key words: micro-Fourier transform infrared spectrometer; light-weight grid beam splitter; spectrum reconstruction

微型傅立叶变换光谱仪的优化设计与实验研究

赵 云[1,2],吕金光[1*],秦余欣[1],陶 金[1],梁中翥[1],王维彪[1],尼启良[1],孟德佳[1],梁静秋[1*]
(1. 中国科学院长春光学精密机械与物理研究所 应用光学国家重点实验室,吉林 长春 130033;
2. 中国科学院大学,北京 100049)

摘要: 为了实现傅立叶变换光谱仪的微型化与轻量化,设计了轻型栅条分束器结构,代替传统的平行平板分束器,分析了

收稿日期: 2019-02-28; **修订日期:** 2019-03-20
基金项目: 国家自然科学基金资助项目(No. 61627819, No. 61575193, No. 61805239, No. 61727818, No. 61735018);吉林省科技发展计划(No. 20190303063SF, No. 20180201024GX, No. 20150520101JH, No. 20170204077GX, No. 20190101012JH, No. 20160204064GX);中国科学院青年创新促进会基金(No. 2018254, No. 2014193);吉林省中青年科技创新领军人才及团队项目(No. 20190101012JH);应用光学国家重点实验室开放基金
National Natural Science Foundation (No. 61627819, No. 61575193, No. 61805239, No. 61727818, No. 61735018); Jilin Province Science and Technology Development Plan (No. 20190303063SF, No. 20180201024GX, No. 20150520101JH, No. 20170204077GX, No. 20190101012JH, No. 20160204064GX); Jilin Province Young and Middle-aged Science and Technology Innovation Leaders and Team Project (No. 20190101012JH); National Fund for Applied Optics Open Fund

轻型栅条分束器的栅棱对光谱复原的影响，提出了制作误差容限。对微型傅立叶变换光谱仪进行了建模仿真，得到了轻型栅条分束器的最佳结构。通过系统仿真进行光谱反演，得到了复原光谱，并计算了轻型栅条分束器引入的光谱误差。完成了原理样机的搭建与调试，得到了实际系统的复原光谱，证明了微型化系统的可行性。该微型化系统相对于传统傅立叶变换光谱仪，具有体积小，稳定性好的优点，可用于在线监测。

关　键　词: 微型傅立叶变换红外光谱仪; 轻型栅条分束器; 光谱复原
中图分类号: 0436　　**文献标识码:** A　　doi: 10.3788/CO.20201302.0411

1 Introduction

At present, Fourier Transform Infrared Spectrometer (FTIRS) is urgently needed in many fields, such as environment, security, meteorology, space detection, gas distribution detection in Unmanned Aerial Vehicle (UAV), military analysis, criminal technology, and anti-terrorism and chemical defense [1-6]. The application of traditional time-modulated FTIRS to online monitoring is limited to some extent due to its moveable parts, complex structure, large volume, and high requirements for transportation and operating environments [7-9]. To solve this problem, micro-FTIRS has attracted researcher's attention.

The micro-FTIRS based on multistage micro-mirror interference system uses two orthogonal multistage micro-mirrors instead of the moving mirror structure of time-modulated FTIRS, uses a light-weight grid beam splitter structure instead of the traditional parallel plate beam splitter, which simplifies the instrument structure and reduces the volume and weight of the instrument by a large margin.

In this paper, a light-weight grid beam splitter made of silica-based etched structure is designed, the optimal structure of the grid beam splitter is obtained through modeling and simulation, and the influence of the grid edge on spectrum restoration is analyzed. Finally, an experimental platform is built to test the beam-splitting effect of the grid beam splitter in the optical system. Based on the platform, the spectral inversion is completed. To obtain the recovered spectrogram. By applying this structure, we significantly reduce the volume and weight of the instrument, realizing the miniaturization of FTIRS.

2 Principle of system operation

The operating principle of micro-FTIRS is shown in Fig. 1. The system mainly consists of infrared light source, collimating system, and high-order multistage micro-mirror, light-weight grid beam splitter, low-order multistage micro-mirror, beam-shrinking system, infrared detector and other components. The infrared source is located at the focal point of the collimating system. The Optical Path Difference (OPD) is generated by two static multistage micro-mirrors orthogonal to each other with different step heights. The grid beam splitter is 45° to the two multistage micro-mirrors respectively. The beam-shrinking system is a double-telecentric optical path, and its object plane coincides with the high-order and low-order multistage micro-mirrors. The infrared cooled detector is located on the image plane of the beam-shrinking system.

The operating principle of this FTIRS is as follows. After being collimated by the collimation system, the light from the infrared source is divided into two beams of coherent light with equal intensity by the grid beam splitter. The two beams are incident to two multistage micro-mirrors respectively. Then the two reflected beams interfere with each other and converge through a beam-shrinking system. Finally, an interference pattern is obtained by using a detector.

Both of the two multistage micro-mirrors have N stages, the step height of low-order is d, and the step height of high-order is Nd. Therefore, the system can obtain $N \times N$ sampling domains with the sampling interval of $\kappa = 2d$.

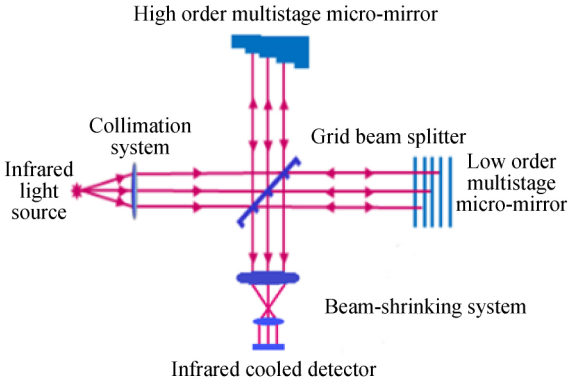

Fig. 1　Schematic diagram of working prinaple for micro-FTIRS

图 1　微型 FTIRS 工作原理图

If the step ordinal of the low-order multistage micro-mirror is x, and the step ordinal of the high-order multistage micro-mirror is y, then the OPD δ corresponding to the sampling domain (x, y) will be

$$\delta(x, y) = 2(Ny - x)d. \tag{1}$$

Therefore, an $N \times N$ OPD sampling array is formed in the interference light field, and the sampling ordinal of the p^{th} OPD is $p = Ny - x$. According to the principle of Fourier transform, the function of interferogram pixel intensity is expressed as [8]

$$I[p(x, y)] = \int_{-\infty}^{\infty} B(v) \exp[2\pi v \delta(x, y)] \, \mathrm{d}v, \tag{2}$$

where $v = 1/\lambda$ is the wave number of light source, and $B(v)$ is the power spectrum density of light. By applying the discrete Fourier transform to equation (2), the spectral information of the light source can be obtained

$$B(v_i) = \sum_{p=-n}^{N^2-n} I(p) \exp\left(-\mathrm{j}\frac{2\pi np}{N^2}\right), \tag{3}$$

where $n = 0, 1, \cdots\cdots, N^2 - 1$; $p = -n, \cdots, 0, \cdots, N^2 - n$; N^2 is the number of shares of incident light divided by the multistage micro-mirror; and $v_i = n/(2dN^2)$ is the discrete wave number.

3　System design and simulation

3.1　Design of light-weight grid beam splitter

Beam splitter is one of the key optical components in the micro-FTIRS. The current traditional FTIRS beam splitter mainly consists of a cubic prism structure and a parallel plate structure, both with a very large volume and weight, which severely limit the miniaturization and light weight of FTIRS.

The miniaturization of beam splitter is one of the key efforts of the FTIRS miniaturization. To structurally reduce the volume and weight of this device and ensure the flatness and surface roughness of beam splitter, we design a light-weight grid beam splitter supported by grid edges. The beam splitter has a window thickness of 0.34 mm and a weight of only about 4% of that of a parallel plate splitter. Therefore, the volume and weight of the beam splitter are effectively reduced, which is beneficial to the miniaturization and lightweight of the spectrometer. In terms of material, the splitter windows and grid edges of the grid beam splitter are of the same material. For the micro-FTIRS in the middle-wave infrared spectrum, we chose monocrystalline silicon as the material of splitter windows and grid edges, and used the Micro-Electro-Mechanical System (MEMS) technology to make a light-weight grid beam splitter through etching. By making full use of the characteristics of monocrystalline silicon, such as high hardness and difficult deformation, monocrystalline silicon grid beam splitter can be fabricated by the MEMS technology with high-precision microstructure processing capacity. Therefore, it has high structural precision, good conformity and high surface figure accuracy and surface finish.

In the design of light-weight grid beam splitter, the structural parameters of grid edges and splitter windows shall match the structures of multistage micro-mirrors and detector in the optical system. The grid edges shall play a supporting role without affecting the spectrum recovery due to too many edges. For the static interference system with multistage micro-mirrors (40 × 40 array), we designed two types of grid beam splitter structure: 10-period type and 20-period type. For example, a 10-period grid beam splitter is composed of 10 splitter windows and 9 grid edges. Each splitter window corresponds to 4 rows of steps of the multi-stage micro-mirrors and 16 rows of pixels of the detector. To avoid the loss of interference image information, the bottom width of grid edges is required to be less than 1/4 of the step width of multistage micro-mirrors. In the size of 40 mm × 56.56 mm, the grid beam splitter is made of monocrystalline silicon by using the anisotropic etching technique. Its lateral etching slope is $\Phi = 54.74°$, the upper surface width of its grid edges is $W = 10$ μm, its edge height is $H = 160$ μm, and its bottom width is $L = 236.6$ μm, as illustrated in Fig. 2.

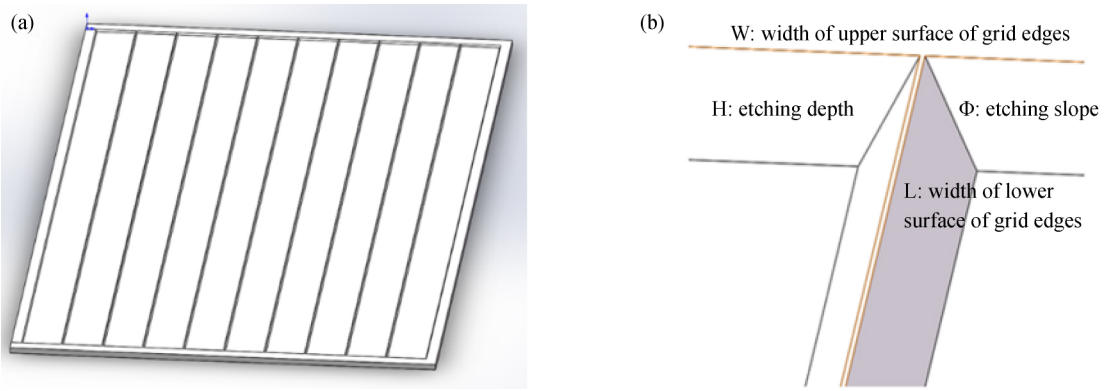

Fig. 2 (a) 10-period grid beam splitter and (b) its partial enlargement.

图 2 (a) 10 周期轻型栅条分束器及其(b) 局部放大图

In the fabrication process of this grid beam splitter, the error of etching depth will affect the distribution of OPDs, thus affecting the spectrum recovery. A 10-period grid beam splitter is taken as an example for analysis. The profile of a single splitter window is shown in Fig. 3. Among them, $b(u)$ is thickness of the u^{th} splitter window; m_1 is incident light; m_2 is emitting light; D is propagation distance of light in the grid beam splitter.

According to the law of refraction, the angle of refraction can be obtained as

$$\theta' = \arcsin\left(\frac{\sin\theta}{\eta}\right), \tag{4}$$

where η is the refractive index of silicon at the thickness of 4 μm, $\eta = 3.4$; and θ is the incident angle of light, $\theta = 45°$. So, $\cos\theta' = 0.98$.

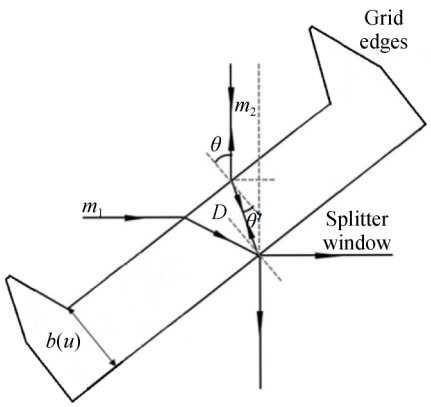

Fig. 3 Profile of a single beam splitter window

图 3 单个分束窗的剖面示意图

Propagation distance of light in the grid beam splitter is

$$D = 2\eta \frac{b(u)}{\cos\theta'} = 6.96b(u). \quad (5)$$

If $\Delta b(u)$ is the maximum thickness error, then the maximum error of optical path will be $6.96\ \Delta b(u)$. In order to evaluate the error between real recovery spectrum and ideal recovery spectrum, we define Spectral Construction Error (SCE) as:

$$SCE = \frac{\sum_{n=0}^{u} |B_{\text{real}}(v_i) - B_{\text{ideal}}(v_i)|}{\sum_{n=0}^{u} B_{\text{ideal}}(v_i)}, \quad (6)$$

where $B_{\text{real}}(v_i)$ is real recovery spectrum, and $B_{\text{ideal}}(v_i)$ is ideal recovery spectrum. By setting different $\Delta b(u)$ values, the graph of relation between $\Delta b(u)$ and *SCE* can be obtained.

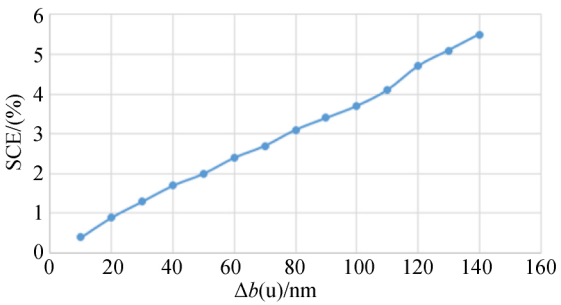

Fig. 4　Relational graph between the thickness error of splitter window and the SCE

图 4　分束窗厚度误差与 SCE 的关系曲线图

It can be seen from Fig. 4 that, when the SCE is 5%, $\Delta b(u)$ is about 125 nm, that is, the allowed maximum thickness error of real splitter window is 125 nm.

3.2　Modeling and simulation

Firstly, each key component in the system is modeled by using the ray-tracing software. As shown in Fig. 5, the compensation plate, which has the same material and structure as grid beam splitter, is placed close to the beam splitter as mirror image. One side of the grid beam splitter is evaporated with half-reflection half-transmission film and the other side is evaporated with infrared anti-reflection film. Both sides of the compensation plate are evaporated with infrared antireflection films. The high-order multistage micro-mirror is placed as mirror position of the low-order multistage micro-mirror relative to the beam splitter.

Parallel-plate beam splitter is used as an ideal structure for the ray tracing and spectral inversion of ideal beam splitter and light-weight grid beam splitter. Through simulation, the influence of light-weight grid beam splitter on spectrum recovery is calculated to obtain the results shown in Fig. 6(Color online).

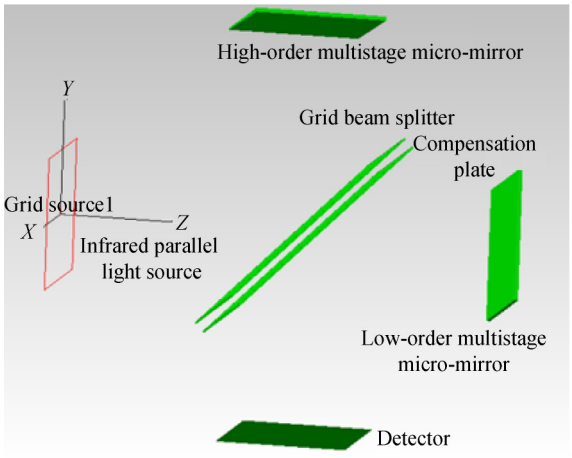

Fig. 5　System modeling diagram

图 5　系统建模图

It can be seen that the presence of grid edges will increase the stray light and affect the spectrum recovery. The distance between high-order/low-order multistage micro-mirror and grid beam splitter is increased to reduce the stray light entering the system. The simulation results are shown in Fig. 7.

It can be seen from Fig. 7 that when the high-order/low-order multistage micro-mirror is 50 mm away from the center of grid beam splitter, the light flux tends to be stable, indicating that most of the stray light will no longer enter the system. Further increasing the distance can reduce more stray light, but can not meet the goal of system miniaturization. Taking the above factors into consideration, the distance between high-order/low-order multistage micro-mirror and grid beam splitter is set as 50 mm.

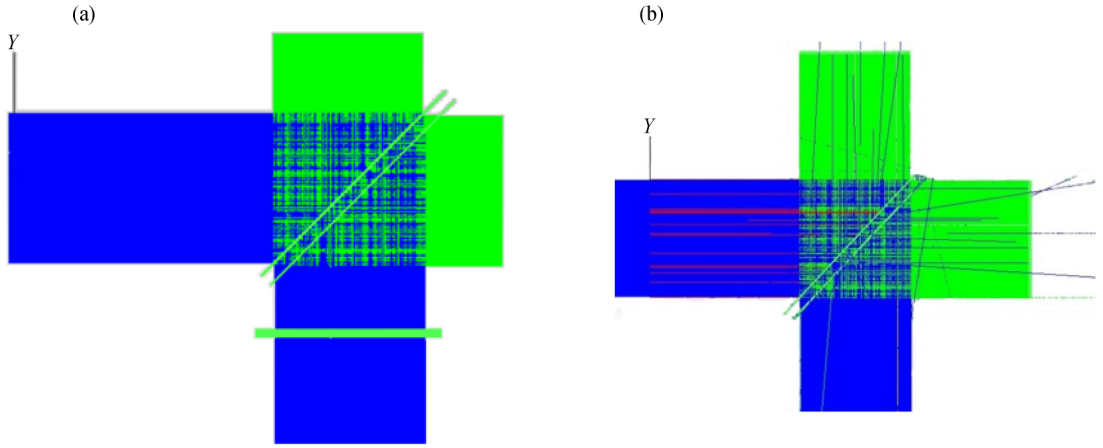

Fig. 6 FTIRS ray tracing with (a) ideal beam splitter and with (b) light-weight grid beam splitter

图 6 (a) 采用理想分束器和(b) 采用轻型栅条分束器得到的 FTIRS 光线追迹图

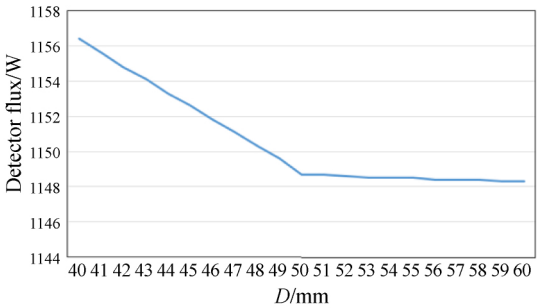

Fig. 7 Relationship between the detector flux and the position of multistage micro-mirror

图 7 探测器光通量与多级微反射镜位置关系图

The collection of interference patterns and the spectrum recovery is completed in the optical simulation software. Three narrow-band light sources, whose central wavelengths are 4.78 μm, 4.19 μm and 3.84 μm respectively, are set. A thin-parallel-plate beam splitter is used as the ideal structure to recover the spectrum of grid beam splitter through simulation, as shown in Fig. 8 (Color online). To be specific, Fig. 8(a) is the ideal recovery pattern of thin parallel plate structure. Since the light reflected by high-order/low-order multistage micro-mirror is coherent light, alternately dark and bright interference fringes appear on the target surface of the detector, and the interference pixels are independent from each other. Fig. 8(b) is the interference pattern with the presence of grid influence. The stray light brought by the reflection and refraction of grid edges smears out the fringe boundary, reduces the light intensity of each interference pixel, and causes the presence of light flux even outside the interference area. Fig. 8(c) is the ideal interference sampling diagram. Fig. 8(d) is the interference sampling diagram with the presence of grid influence. Fig. 8(e) is the ideal reconstructed spectrum. It can be seen that three narrow-band spectra appear at the wave numbers 2 090, 2 380, and 2 600. This matches the original setting of light source. Fig. 8(f) is the recovery spectrum with the presence of grid influence. Compared with ideal recovery spectrum, the recovery spectrum in Fig. 8(f) has certain background noise. According to the 10-period grid beam splitter structure designed in this paper, the SCE of actual recovery spectrum is calculated to be 2.91%, less than 5%, and thus meets the design requirement.

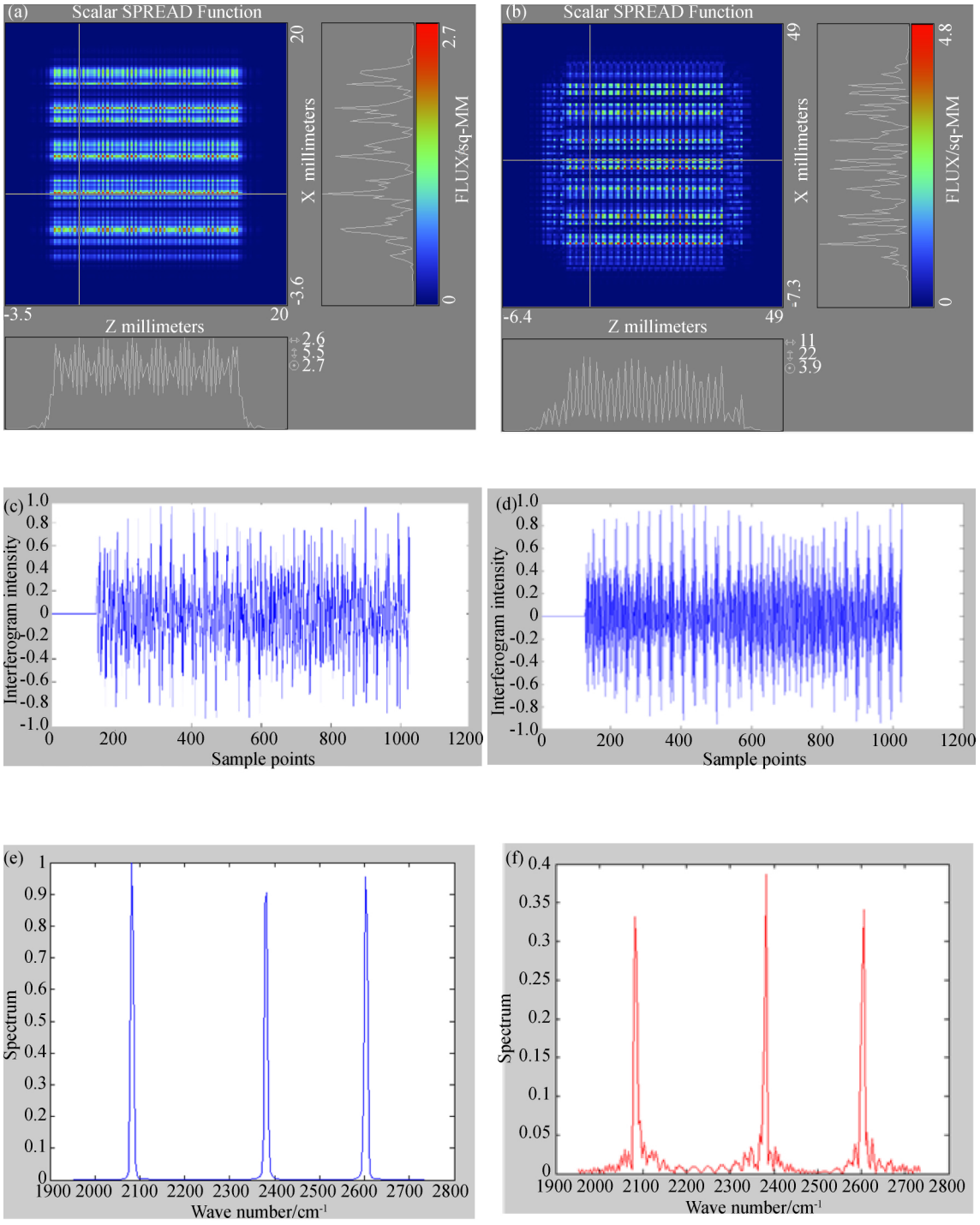

Fig. 8　System simulation results. (a) Ideal interferogram image; (b) interferogram image with beam splitter; (c) ideal interferogram sampling sequence; (d) interferogram sampling sequence with beam splitter; (e) ideal recovered spectrum; (f) recovered spectrum with beam splitter

图 8　系统仿真结果。(a) 理想干涉图像; (b) 带有栅条分束器的干涉图像; (c) 理想干涉图采样序列; (d) 带有栅条分束器的干涉采样序列; (e) 理想复原光谱; (f) 带有栅条分束器的复原光谱

4 Device fabrication and test analysis

The light-weight grid beam splitter is fabricated by anisotropic wet etching process, as shown in Fig. 9(Color online)[10-11]. The specific steps are as follows: (a) growing SiO_2 film on a silicon wafer; (b) photoresist spin-coating; (c) exposure and development; (d) etching and obtaining a SiO_2 mask pattern; (e) wet etching with KOH solution; (f) removal of photoresist; (g) removal of SiO_2.

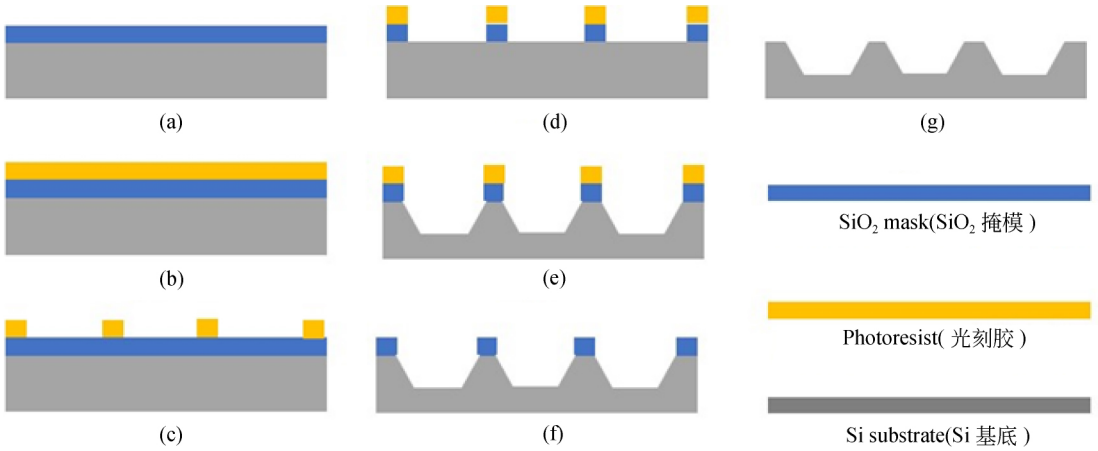

Fig. 9 Fabrication process of silicon-based etched grid beam splitter

图 9 硅基腐蚀轻型栅条分束器的制作流程

The 10-period and 20-period grid beam splitters are selected for experimental study. By using the process flow shown in Fig. 9, the real splitters are obtained as shown in Fig. 10.

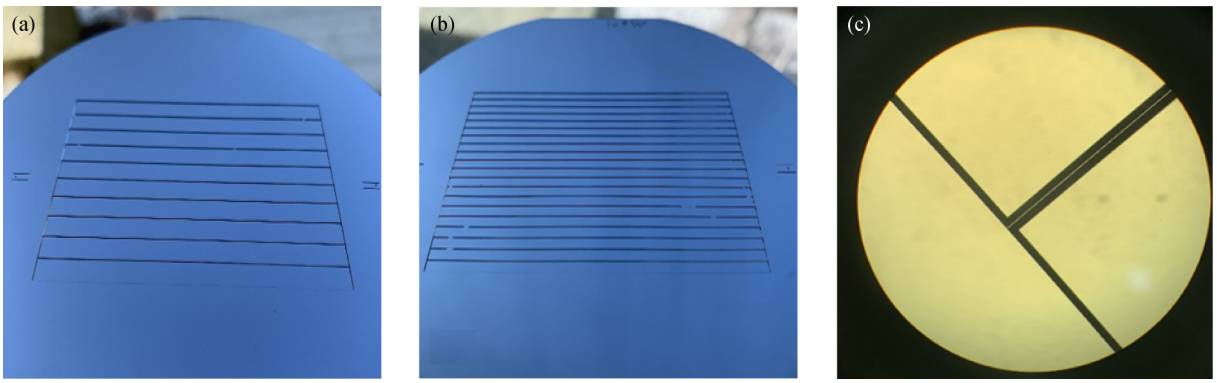

Fig. 10 Prototype of grid beam splitter; (a) 10-period grid beam splitter; (b) 20-period grid beam splitter; (c) microscopic topography

图 10 栅条分束器实物图。(a) 10 周期栅条分束器; (b) 20 周期栅条分束器; (c) 显微镜图

The depth error and uniformity error generated during the fabrication of grid beam splitter will introduce additional OPD and distort the recovery spectrum. The maximum etching depth differences of 10-period and 20-period grid beam splitters, as shown in Fig. 11, are measured by a step profiler. For 10-period grid beam splitter, the mean etching depth is 161.522 μm, the standard deviation of etching depth is 37.58 nm, and the maximum depth difference is 48 nm.

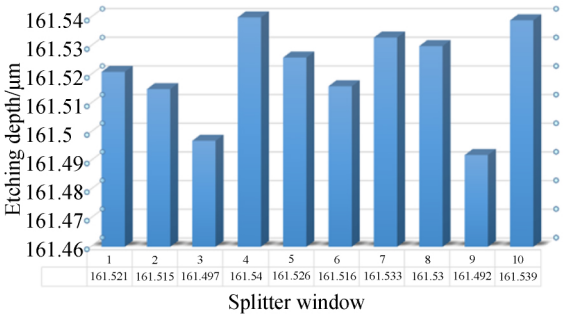

Fig. 11　Etching depth test result of 10-period grid beam splitter

图 11　10 周期轻型栅条分束器腐蚀深度测试结果

Fig. 12 shows the etching depth test result of 20-period grid beam splitter. For this beam splitter, the calculated mean etching depth is 159.774 μm, the standard deviation of etching depth is 31.24 nm, and the maximum depth difference is 38 nm. The maximum etching depth differences of the two grid beam splitters are both less than the maximum amount allowed for $\Delta b(u)$, namely 125 nm, so the influence of etching depth error of grid beam splitter on spectrum recovery can be ignored.

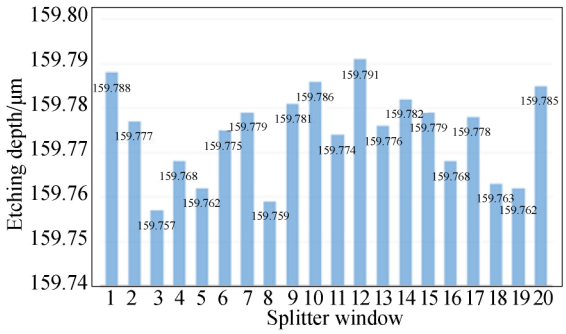

Fig. 12　Etching depth test result of 20-period grid beam splitter

图 12　20 周期轻型栅条分束器腐蚀深度测试结果

5　Experiment results and discussion

The technique of laser reference positioning is used to install and adjust the test devices and build an experimental platform, as shown in Fig. 13. The step heights of high-order and low-order multistage micro-mirrors are 20 μm and 0.625 μm respectively. The detector is a middle-infrared focal plane detector array with 320 × 256 detection pixels, each of which is 30 μm × 30 μm.

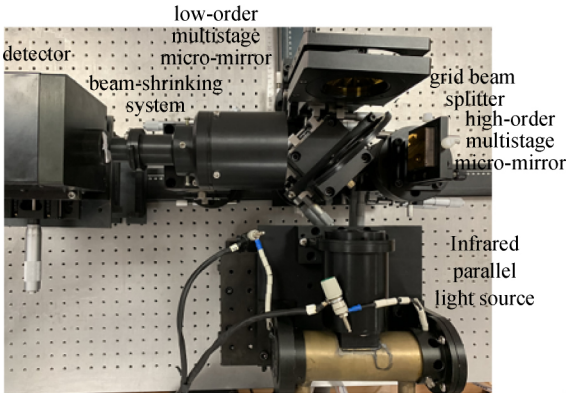

Fig. 13　Experimental prototype

图 13　实验原型机图片

The Figs. 14(a) and 14(b) are the interference patterns obtained by using 10-period and 20-period grid beam splitters respectively, and the Figs. 14(c) and 14(d) are their interference sampling diagrams respectively. Through noise reduction, apodization, DC component removal and phase correction, the corrected interference sampling diagrams are obtained, as shown in Figs. 14(e) and 14(f). Through the Fourier transform, the recovery spectrum is obtained, as shown in Fig. 15. In the Fig. 15, the curve 1 is the light source spectrum, the curve 2 is the recovery spectrum of 10-period grid beam splitter, and the curve 3 is the recovery spectrum of 20-period grid beam splitter.

As can be seen from Fig. 15, the 10-period grid beam splitter has fewer periods and less shading of light, so it contains less noise and produces a smaller impact on spectrum recovery. In contrast, due to the existence of more grid edges, stray light is increased and the spectrum distorted in the 20-peri-

od grid beam splitter. According to the calculation result, the SCE of 10-period grid beam splitter is 3.9% and that of 20-period grid beam splitter is 6.1%. Since a light-weight grid beam splitter with too few periods can't ensure the surface figure accuracy, the 10-period grid beam splitter is a good fit for the system requirements.

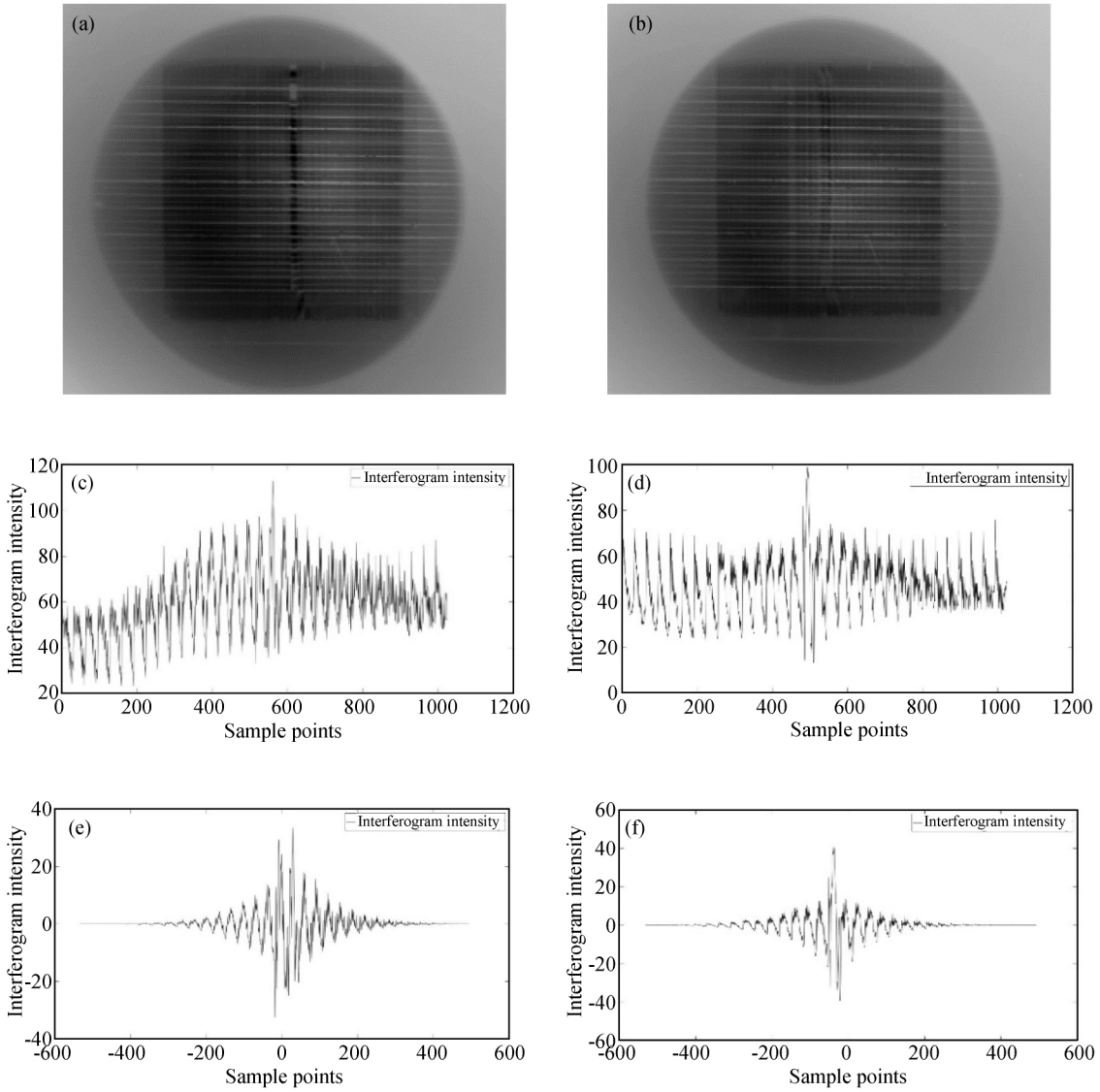

Fig. 14 (a) Interference fringe pattern of 10-period grid beam splitter; (b) interference fringe pattern of 20-period grid beam splitter; (c) interference sampling diagram of 10-period grid beam splitter; (d) interference sampling diagram of 20-period grid beam splitter; (e) interference sampling diagram of 10-period grid beam splitter after correction; (f) interference sampling diagram of 20-period grid beam splitter after correction

图 14 (a) 10 **周期栅条分束器干涉条纹图**; (b) 20 **周期栅条分束器干涉条纹图**; (c) 10 **周期栅条分束器干涉采样图**; (d) 20 **周期栅条分束器干涉采样图**; (e) **校正后** 10 **周期栅条分束器干涉采样图**; (f) **校正后** 20 **周期栅条分束器干涉采样图**

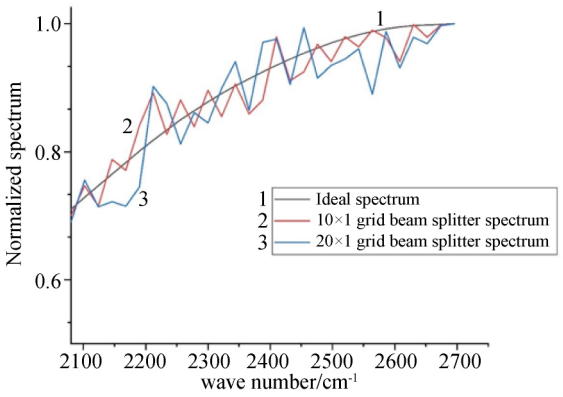

Fig. 15　Ideal spectrum and restored spectra of lo-period and 20-period grid beam splitters

图 15　理想光谱与 2 种栅条分束器的复原光谱图

6　Conclusion

In this paper, a light-weight beam splitter with silicon-based grid structure made by anisotropic etching technique is proposed to replace the traditional beam splitter of spatially modulated FTIRS. 10-period and 20-period grid beam splitters were designed and processed, and the influence of their errors on spectrum recovery was analyzed. The beam-splitting effect of two kinds of grid beam splitters with different structures was measured by experiment to obtain the light source spectrum. The experimental results showed that the instrument could meet the application requirements of the micro FTIRS and realize the miniaturization of the interference system. In future experiments, a new kind of multistage micro-mirror with the increased step width of the corresponding grid edges can be made to reduce the influence of grid edges on spectrum reconstruction.

——中文对照版——

1　引　言

目前，环境、安全、气象、空间探测、无人机载气体分布探测、军事分析、刑事技术以及反恐防化等诸多领域对傅立叶变换红外光谱仪(Fourier Transform Infrared Spectrometer, FTIRS) **提出了十分迫切的需求**[1-6]**。传统的时间调制型** FTIRS **由于含有可动部件，结构较为复杂，体积较大，对运输及使用环境要求较高，使其在在线监测等方面的应用受到一定限制**[7-9]**。为了解决这一问题，微型** FTIRS **引起了人们的关注。**

采用多级微反射镜干涉系统的微型 FTIRS**，用两个正交放置的多级微反射镜取代时间调制型** FTIRS **的动镜结构，并使用轻型栅条分束器代替传统平行平板分束器，简化了仪器结构，使仪器的体积与重量明显下降。**

本文设计了一种硅基腐蚀结构制作的轻型栅条分束器，通过建模仿真得到了轻型栅条分束器的最佳结构，分析了栅棱对于光谱复原的影响。最后完成了实验平台的搭建，测试了栅条分束器在光学系统中的分束效果，完成了光谱反演，得到了实际系统的复原光谱图，实现了 FTIRS **的微型化，使仪器体积与重量明显下降。**

2　系统工作原理

微型傅立叶变换红外光谱仪的工作原理图如图 1 **所示，系统主要由红外光源、准直系统、高阶多级微反射镜、轻型栅条分束器、低阶多级微反射镜、缩束系统和红外探测器等组成。红外光源位于准直系统的焦点处。由两个正交放置的具有不同阶梯高度的静态多级微反射镜产生光程差，轻型栅条分束器与两个多级微反射镜分别呈** 45°**放置。缩束系统为双远心光路，其物面与高低多级微反射镜重合，红外制冷探测器位于缩束系统像面处。**

本文设计的 FTIRS **的工作原理为：红外光源发出的光经准直系统准直后，被轻型栅条分束器分成两束强度相等的相干光，分别入射到两个多**

级微反射镜上，两束反射光相互干涉，通过缩束系统汇聚，最后用探测器测得干涉图。

两个多级微反射镜的级数均为 N，阶梯高度均为 d，即低阶多级微反射镜的阶梯高度为 d，高阶多级微反射镜的高度为 Nd，因此系统可以获得采样间隔为 $\kappa = 2d$ 的 $N \times N$ 个采样定域。设低阶多级微反射镜的阶梯序数为 x，高阶多级微反射镜的阶梯序数为 y，则采样定域(x,y)所对应的光程差 δ 为:

$$\delta(x,y) = 2(Ny - x)d. \tag{1}$$

因此，在干涉光场构成一个 $N \times N$ 的光程差采样阵列，第 p 个光程差采样序数为 $p = Ny - x$。根据傅立叶变换原理，干涉图元强度的函数表达式为[8]:

$$I[p(x,y)] = \int_{-\infty}^{\infty} B(v)\exp[2\pi v\delta(x,y)]\,\mathrm{d}v, \tag{2}$$

式中 $v = 1/\lambda$，为光源波数，$B(v)$ 为光的功率谱密度。对式(2)进行离散傅立叶变换，可以得到光源的光谱信息:

$$B(v_i) = \sum_{p=-n}^{N^2-n} I(p)\exp\left(-\mathrm{j}\frac{2\pi np}{N^2}\right), \tag{3}$$

其中，$n = 0,1,\cdots\cdots,N^2-1$，$p = -n,\cdots,0,\cdots,N^2-n$，$N^2$ 为多级微反射镜将入射光所分的份数，$v_i = n/(2dN^2)$ 是离散波数。

3 系统设计与模拟仿真

3.1 轻型栅条分束器设计

分束器是微型傅立叶变换光谱仪的关键光学元件之一。目前传统 FTIRS 的分束器主要有立方棱镜结构和平行平板结构，两种结构的体积和重量都很大，严重限制了 FTIRS 的微小型化与轻量化。

分束器的微型化是傅立叶变换红外光谱仪微型化的关键之一。设计原则是: 在结构上，既要减小该器件的体积和重量，又要保证分束器的平面度和表面粗糙度。本论文设计了一种由栅棱支撑的轻型栅条分束器，其分束窗窗口厚度为 0.34 mm，分束器重量仅为平行平板分束器的 4% 左右，因此有效减小了分束器的体积和重量，有利于光谱仪的微小型化和轻量化。在材料方面，轻型栅条分束器的分束窗与栅棱选择同种材料。针对中波红外谱段的微型 FTIRS，选择单晶硅作为分束器的分束窗与栅棱材料，采用微机电系统(Micro-Electro-Mechanical System，MEMS)腐蚀制作轻型栅条分束器。单晶硅结构轻型栅条分束器充分利用了单晶硅材料硬度大，不易形变的特点，可以通过具有高精度微结构加工能力的 MEMS 技术进行制作，结构精度高，一致性好，较好地保证了器件的面形精度及表面光洁度。

在轻型栅条分束器的设计中，栅棱及分束窗的结构参数需与光学系统中多级微反射镜及探测器的结构相匹配，栅棱既要起到支撑作用，数量又不能过多，数量过多会影响光谱复原。针对 40 × 40 阵列的多级微反射镜静态干涉系统，本文设计了 10 周期与 20 周期的两种轻型栅条分束器结构。以 10 周期轻型栅条分束器为例，其由 10 个分束窗和 9 个栅棱组成，每个分束窗对应多级微反射镜的 4 行阶梯，对应探测器的 16 行像素。为了不丢失干涉图像的信息，要求栅棱底部宽度小于多级微反射镜阶梯宽度的 1/4。轻型栅条分束器的尺寸设计为 40 mm × 56.56 mm，采用单晶硅各向异性腐蚀技术制作，侧向腐蚀斜率为 $\Phi = 54.74°$，栅棱上表面的宽度为 $W = 10$ μm，棱高为 $H = 160$ μm，底部宽度为 $L = 236.6$ μm。如图 2 所示。

在轻型栅条分束器的制作过程中，腐蚀深度误差会影响光程差的分布，从而对光谱复原产生影响。以 10 周期的轻型栅条分束器为例进行分析，单个分束窗的剖面示意图如图 3 所示。其中，$b(u)$ 为 u 阶分束窗的厚度; m_1 为入射光; m_2 为出射光; D 为光在轻型栅条分束器中的传播距离。

根据折射定率，可以得到折射角为:

$$\theta' = \arcsin\left(\frac{\sin\theta}{\eta}\right), \tag{4}$$

其中，$\eta = 3.4$，是硅在 4 μm 处的折射率，$\theta = 45°$ 是入射光线的入射角，可得 $\cos\theta' = 0.98$，则有

$$D = 2\eta \frac{b(u)}{\cos\theta'} = 6.96b(u). \quad (5)$$

设 $\Delta b(u)$ 为最大厚度误差，则最大光程误差为 $6.96\Delta b(u)$。为了评价实际复原光谱和理想复原光谱之间的误差，定义重构光谱误差（Spectral Construction Error，SCE）为：

$$SCE = \frac{\sum_{n=0}^{u} |B_{\text{real}}(v_i) - B_{\text{ideal}}(v_i)|}{\sum_{n=0}^{u} B_{\text{ideal}}(v_i)}, \quad (6)$$

其中 $B_{\text{real}}(v_i)$ 为实际复原光谱，$B_{\text{ideal}}(v_i)$ 为理想复原光谱，通过设置不同的 $\Delta b(u)$ 值，得到 $\Delta b(u)$ 与 SCE 的关系曲线图。

由图 4 可以看出，当 SCE 为 5% 时，$\Delta b(u)$ 约为 125 nm，即实际制作的轻型栅条分束器的分束窗的最大厚度误差允许量为 125 nm。

3.2　建模与仿真

首先用光线追迹软件对系统各个关键器件进行建模，如图 5 所示，补偿板与轻型栅条分束器材料相同，结构相同，补偿板紧靠分束器，两者呈镜像放置。在轻型栅条分束器上一面蒸镀半反半透膜，另一面蒸镀红外增透膜；补偿板两面均蒸镀红外增透膜。高阶多级微反射镜与低阶多级微反射镜相对轻型栅条分束器呈镜像放置。

将采用平行平板分束器的情况作为理想状态，对理想状态下的分束器与轻型栅条分束器分别进行光线追迹与光谱反演，通过模拟仿真计算轻型栅条分束器对复原光谱的影响，得到的结果如图 6（彩图见期刊电子版）所示。

可以看出栅棱的存在会增加杂散光，影响光谱复原。通过同时增加高低多级微反射镜与轻型栅条分束器之间的距离，以减少进入系统的杂散光，仿真结果如图 7 所示。

由图 7 可知，当高低多级微反射镜距离轻型栅条分束器中心 50 mm 时，光通量趋于稳定。这说明此时大部分杂散光不再进入系统，继续增大距离虽可进一步减少杂散光，但不符合系统微型化的目标，综合考虑以上因素，将高低多级微反射镜与轻型栅条分束器的距离设置为 50 mm。

在光学仿真软件中完成干涉图的采集，并使用仿真软件完成光谱复原。光源设置为 3 个窄带光源，其中心波长分别为 4.78、4.19、3.84 μm，使用薄平行平板分束器作为理想结构，通过仿真得到轻型栅条分束器的光谱复原图，结果如图 8（彩图见期刊电子版）所示。其中，图 8（a）为薄平行平板结构的理想干涉图，由于高低多级微反射镜反射的光为相干光，因此在探测器靶面上呈现出明暗相间的干涉条纹，且各个干涉像元相互独立。图 8（b）为存在栅条影响的干涉图，由于栅棱的反射与折射引入了杂散光，使条纹的分界不明显，降低了各个干涉像元的光强度，且干涉区域之外也出现了光通量，图 8（c）为理想干涉采样图，图 8（d）为存在栅条影响的干涉采样图，图 8（e）为理想复原光谱，可以看到在 2 090、2 380、2 600 波数处共出现 3 条窄带光谱，与最初设置的光源相符合，图 8（f）为存在栅条影响的复原光谱，与理想复原光谱相比，存在栅条影响的复原光谱出现了一定的背景噪声。根据本文设计的 10 周期轻型栅条分束器结构，计算出实际复原光谱的 SCE 为 2.91%，小于 5%，符合设计要求。

4　器件制作与测试分析

采用各向异性湿法腐蚀工艺制作轻型栅条分束器，具体工艺流程如图 9（彩图见期刊电子版）所示[10-11]。具体步骤为：（1）在硅片上生长 SiO_2 薄膜；（2）旋涂光刻胶；（3）曝光与显影；（4）腐蚀并得到 SiO_2 掩模图形；（5）使用 KOH 溶液进行湿法腐蚀；（6）去除光刻胶；（7）去除 SiO_2。

选取 10 周期与 20 周期轻型栅条分束器进行实验研究，根据图 9 所示的工艺流程，得到实物如图 10 所示。

由于在轻型栅条分束器制作过程中产生的深度误差及均匀性误差会引入附加光程差，使复原光谱失真，故使用台阶仪分别测量了 10 周期与 20 周期轻型栅条分束器的最大腐蚀深度差，如图 11 所示。得到 10 周期轻型栅条分束器的腐蚀深度均值为 161.522 μm，标准差为 37.58 nm，最大深度差为 48 nm。

图 12 为 20 周期的轻型栅条分束器的深度测试结果，计算得到其腐蚀深度均值为 159.774 μm，标准差为 31.24 nm，最大深度差为 38 nm。两种轻型栅条分束器腐蚀深度的最大差值均小于 $\Delta b(u)$ 的最大允许量 125 nm。由此可知，轻型栅条分束器的腐蚀深度误差对光谱复原的影响可以

忽略。

5 实验结果与讨论

利用激光参考定位进行装调，搭建实验平台，如图13所示。高低多级微反射镜的阶梯高度分别为20 μm和0.625 μm。探测器为中红外焦平面探测器阵列，含有320×256个探测像元，单个像元大小为30 μm×30 μm。

图14(a)和图14(b)分别为采用10周期栅条分束器与20周期栅条分束器得到的干涉图，图14(c)和图14(d)分别为它们的干涉采样图。通过降噪、切趾、去除直流分量及相位校正等操作，得到校正后的干涉采样图，如图14(e)和图14(f)所示。进行傅立叶变换，得到复原光谱图，如图15所示，其中曲线1为光源光谱，曲线2为10周期栅条分束器复原光谱，曲线3为20周期栅条分束器复原光谱。

由图15可以看出，10周期栅条分束器的周期少，对光线遮挡也较少，因此包含的噪声较少，对光谱复原影响较小，20周期栅条分束器由于存在较多栅棱，增加了杂散光，使光谱失真。通过计算得到10周期栅条分束器的SCE为3.9%，20周期栅条分束器的SCE为6.1%。若轻型栅条分束器的周期太少，则无法保证面形，而10周期轻型栅条分束器满足系统要求。

6 结 论

本文提出用硅基各向异性腐蚀技术制作的栅条结构轻型分束器取代空间调制傅立叶变换红外光谱仪的传统分束器，设计并加工了10周期与20周期轻型栅条分束器，分析了其误差对于光谱复原的影响。通过实验测试了两种不同结构轻型栅条分束器的分束效果，得到了光源光谱。结果表明：该仪器可以满足微型傅立叶变换光谱仪的应用要求，实现了干涉系统的轻小型化。在未来的实验中，可以制作新型多级微反射镜，增加多级微反射镜上对应栅棱部分的阶梯宽度，以降低栅棱对于光谱复原的影响。

参考文献：

[1] BRACHET F, HÉBERT P J, CANSOT E, *et al*.. Static Fourier transform spectroscopy breadboards for atmospheric chemistry and climate [J]. *Proceedings of SPIE*, 2008, 7100: 710019.

[2] LACAN A, BRÉON F M, ROSAK A, *et al*.. A static Fourier transform spectrometer for atmospheric sounding: concept and experimentalimplementation [J]. *Optics Express*, 2010, 18(8): 8311-8331.

[3] 付建国，梁静秋，梁中翥. 一种静态傅里叶变换红外光谱仪的光学系统分析与设计 [J]. 光学学报，2012，32(2)：0222006.
FU J G, LIANG J Q, LIANG ZH ZH. Analysis and design for the optical system of a static infrared Fourier transform spectrometer [J]. *Acta Optica Sinica*, 2012, 32(2): 0222006. (in Chinese)

[4] 李相贤，徐亮，高闽光，等. 分析温室气体及CO2碳同位素比值的傅里叶变换红外光谱仪 [J]. 光学 精密工程，2014，22(9)：2359-2368.
LI X X, XU L, GAO M G, *et al*.. Fourier transform infrared greenhouse analyzer for gases and carbon isotope ratio [J]. *Opt. Precision Eng.*, 2014, 22(9): 2359-2368. (in Chinese)

[5] WALLRABE U, SOLF C, MOHR J, *et al*.. Miniaturized Fourier transform spectrometer for the near infrared wavelength regime incorporating an electromagnetic linear actuator [J]. *Sensors and Actuators A: Physical*, 2005, 123-124: 459-467.

[6] FENG C, WANG B, LIANG ZH ZH, *et al*.. Miniaturization of step mirrors in a static Fourier transform spectrometer: theory and simulation [J]. *Journal of the Optical Society of America B*, 2011, 28(1): 128-133.

[7] IVANOVE V. Static Fourier transform spectroscopy with enhanced resolving power [J]. *Journal of Optics A: Pure and Applied Optics*, 2000, 2(6): 519-528.

[8] FENG C, LIANG J Q, LIANG ZH ZH. Spectrum constructing with nonuniform samples using least-squares approximation by cosine polynomials [J]. *Applied Optics*, 2011, 50(34): 6377-6383.

[9] 陈少杰，齐向东，巴音贺希格，等. 用于激光诱导等离子体光谱分析的便携式中阶梯光栅光谱仪设计 [J]. 发光学报，2013，34(5)：672-677.

CHEN SH J, QI X D, BAYANHESHIG, *et al.*. A portable echelle spectrograph design for laser-induced breakdown spectroscopy [J]. *Chinese Journal of Luminescence*, 2013, 34(5): 672-677. (in Chinese)

[10] 吕金光，梁静秋，梁中翥，等. 空间调制傅里叶变换红外光谱仪分束器楔形误差分析 [J]. 光学学报，2014，34(10)：1030001.
LV J G, LIANG J Q, LIANG ZH ZH, *et al.*. Analysis of wedge error of beam splitter in spatial modulation Fourier transform infrared spectrometer [J]. *Acta Optica Sinica*, 2014, 34(10): 1030001. (in Chinese)

[11] 李晚侠，卢启鹏，宋源，等. 基于双直角分束器的反射式静态傅里叶光谱仪光学系统 [J]. 光学学报，2017，37(8)：0812004.
LI W X, LU Q P, SONG Y, *et al.*. Reflective static Fourier spectrometer optical system based on double right-angle beam splitter [J]. *Acta Optica Sinica*, 2017, 37(8): 0812004. (in Chinese)

作者简介:

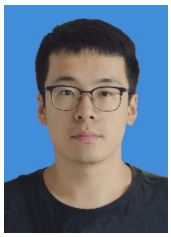

ZHAO Yun (1993—), male, born in Zibo City, Shandong Province. Master degree. In 2016, he obtained the bachelor's degree from Hefei University of Technology. Since 2016, he has been studying for the master degree in the CAS Changchun Institute of Optics, Fine Mechanics and Physics, where he is mainly engaged in the research of optical design. E-mail: 1002803876@qq.com

赵　云(1993—)，男，山东淄博人，硕士研究生，2016 年于合肥工业大学获得学士学位，主要从事光学设计方面的研究。E-mail: 1002803876@qq.com

LV Jin-guang (1984—), male, born in Jiaohe City, Jilin Province. Ph. D. and associate researcher. Mainly engaged in the research of micro optical systems design and optical information processing. E-mail: jinguanglv@163.com

吕金光(1984—)，男，吉林蛟河人，博士，副研究员，2008 年于吉林大学获得学士学位，2013 年于中国科学院长春光学精密机械与物理研究所获得博士学位，主要从事微小光学系统设计与光学信息处理方面的研究。E-mail: jinguanglv@163.com

LIANG Jing-qiu (1962—), female, born in Shenyang City, Liaoning Province. Doctoral supervisor. Mainly engaged in the research of micro optical systems, micro-optical electromechanical systems (MOEMS) and microstructure optics. E-mail: liangjq@ciomp.ac.cn

梁静秋(1962—)，女，辽宁沈阳人，博士，研究员，博士生导师，1984 年于吉林大学获得学士学位，2003 年于中国科学院长春光学精密机械与物理研究所获得博士学位，主要从事微小型光学系统、微光机电系统(MOEMS)及微结构光学方面的研究。E-mail: liangjq@ciomp.ac.cn